Coherent-synchrotron-radiation-free longitudinal shaping of a high-charge electron bunch based on velocity modulation

Zhi Song, Shiyu Zhou, Jianfei Hua,* Yingchao Du, Fei Li, Bo Peng, and Wei Lu†
Department of Engineering Physics, Tsinghua University, Beijing 100084, China

Zhen Wang
Shanghai Advanced Research Institute, Chinese Academy of Sciences, Shanghai 201204, China

(Received 31 October 2023; accepted 8 August 2024; published 12 September 2024)

Beam-driven plasma wakefield acceleration (PWFA) is a promising technique to generate high-energy electron bunches for future electron-positron colliders. Longitudinal shaping of high-charge drive beam is highly desired for achieving high-transformer ratio and loading high-charge witness beam. However, the existing shaping schemes either focused on relatively low-charge bunch shaping or accompanied with significant charge-loss rate (typically over 50%). In this paper, a coherent-synchrotron-radiation-free shaping scheme based on velocity modulation is proposed to generate a high-charge beam with a linearly ramped profile. A >10 kA-peak-current shaped beam containing >50 nC charge with a low charge-loss rate is demonstrated by a start-to-end simulation, and the tunabilities of the beam charge and the peak current, and the robustness of the proposed shaping scheme are also discussed. When loaded by a 3 nC witness beam, a >GV/m accelerating electric field with a transformer ratio larger than 4 can be achieved in a uniform plasma for the shaped drive beam, providing the possibility of high-transformer-ratio PWFA for a high-charge beam.

DOI: 10.1103/PhysRevAccelBeams.27.092801

I. INTRODUCTION

High-luminosity high-energy electron-positron colliders are desirable for fundamental physics studies. It is envisioned that high-charge electron bunches with energy of TeV level are required in the near future. As the accelerating gradient of current radio-frequency (rf) acceleration is typically limited to tens of MV/m by breakdowns, different advanced acceleration techniques have been proposed to provide much higher gradient to make accelerators more compact and cost-effective. One of the promising candidates is the beam-driven plasma wakefield acceleration (PWFA) [1], which have demonstrated accelerating gradient of 1–50 GV/m, narrow energy spread, and high-energy transfer efficiency [2,3]. In PWFA, an ultrarelativistic drive beam (usually an electron bunch) propagating through plasma excites strong wakefield, and a customized witness beam (electron or positron bunch) loaded at a proper phase can be accelerated with high gradient and high quality.

*Contact author: jfhua@tsinghua.edu.cn
†Contact author: weilu@tsinghua.edu.cn

Concerning the requirements of a PWFA-based electron-positron collider, two parameters are of great interest. One is the so-called transformer ratio $R = E_+/E_-$, the ratio of the maximum accelerating field E_+ for the witness beam to the maximum decelerating field E_- within the drive beam. Given the energy loss of the drive beam, a larger R leads to a higher energy gain of the witness beam. To excite a plasma wake with high-transformer ratio ($R > 2$), both the linear and nonlinear theories indicate that a shaped drive beam with an asymmetric current distribution, typically a triangular current profile that rises linearly from head to tail and then drops to zero in a short range, is needed [4–7]. The other parameter of great concern is the charge of the drive beam. For electron-positron colliders, higher-charge beam is desired for improving the luminosity [8]. According to the law of energy conservation, for achieving the acceleration of a high-charge witness beam in a high-transformer-ratio (HTR) acceleration, the charge of drive beam should be at least R times as high as that of witness beam. For a representative set of parameters: energy transfer efficiency from the drive beam to the witness beam of ~30% [3], a witness beam of 3 nC [9], and $R = 4$, several tens of nC for the drive beam is needed.

Various approaches [10] to produce bunches with linearly ramped profiles can be roughly categorized as mask-based shaping [11–17], correlation-based shaping [18–20], self-fields-based shaping [21–23], photocathode laser

shaping [24–27], and shaping by entire beamline optimization [28]. For the high-charge (>10 nC) bunch shaping, most existing methods are accompanied with either high-charge-loss rates (typically over 50% for mask-based shaping), or coherent-synchrotron-radiation (CSR) effects. Under the situation of high-charge cases, the high-charge-loss rate can unavoidably induce severe thermal or radiation issues, while CSR effects can deteriorate the shaping quality, transverse emittance, or slices collimation of the beam. Hence, a high-charge shaping regime with low charge-loss rate and high beam quality is pursed.

In this paper, a compact CSR-free scheme for longitudinal shaping based on velocity modulation is proposed, and its capability of generating high-charge current-shaped bunch with low charge-loss rate is demonstrated via numerical simulations. Based on velocity modulation of a beam at a relatively low energy (several MeV), the longitudinal shaping can be achieved by using a photocathode gun, a following rf cavity and a drift segment. Particles injected into the cavity at different phases will obtain different energy-dependent velocities and finally achieve different longitudinal positions after the drift segment. For a typical bunch generated from the gun, a proper velocity modulation can be introduced by combined manipulations of the amplitude and the phase of the rf cavity, and the target current profile can be produced at the end of the drift.

In the following part of this paper, the shaping scheme based on velocity modulation is illustrated in Sec. II. In Sec. III, a simulation is carried out to verify the generation of a linearly ramped current profile with the charge of over 50 nC. The tunabilities of the beam charge and the peak current, and the robustness of the proposed shaping scheme are discussed in Sec. IV. In Sec. V, the >50 nC shaped bunch is numerically demonstrated to drive a PWFA with a transformer ratio larger than 4, and a summary is made in Sec. VI.

II. SHAPING CONCEPT BASED ON VELOCITY MODULATION

The key point for an effective longitudinal density modulation based on velocity modulation is that the shaping process occurs predominantly at relatively low beam energy (e.g., several MeV), where the bunch velocity not very close to the speed of light. Figure 1(a) shows the sketch of a beamline for the shaping scheme, and the energy chirp is defined to be negative if the bunch head has lower energy than the tail in this paper. The generation of a linearly ramped current profile based on the proposed shaping scheme is simulated by program ASTRA [29] (the space charge effects and wakefield effects are excluded) as an example. Figures 1(b)–1(e) show the longitudinal phase spaces with corresponding current profiles at different locations, respectively. The electron

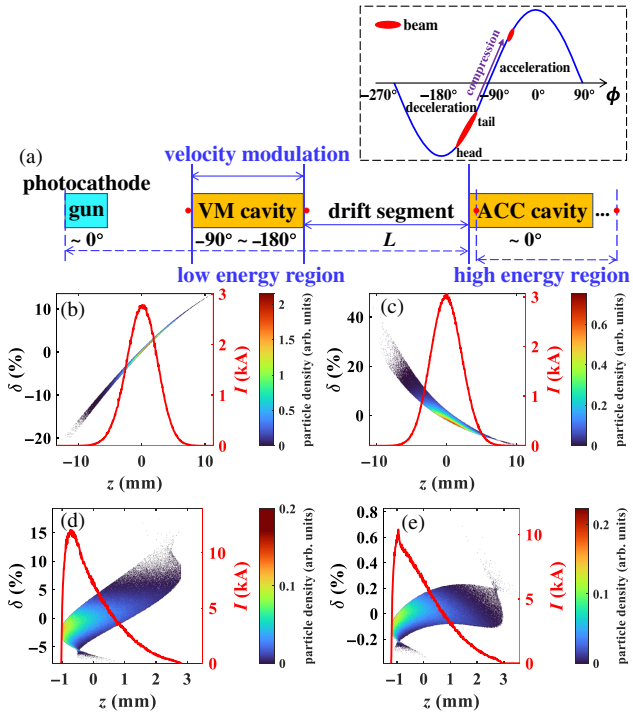

FIG. 1. An illustration of velocity-modulation-based shaping scheme. (a) A sketch of a beamline for the shaping scheme, where the subplot defines the electron phase with respect to the wave. The longitudinal phase spaces with corresponding current profiles at (b) the entrance of VM cavity, (c) the exit of VM cavity, (d) a short distance downstream from the entrance of ACC cavity, and (e) the exit of ACC cavity. The bunch head is at right.

bunch emitted from a photocathode is accelerated to several MeV at the exit of the gun and then drifts to the entrance of VM cavity. VM cavity is utilized for providing an appropriate velocity modulation, i.e., selecting a proper electric field and a proper phase in the range of $(-180°, -90°)$ to impart a negative energy chirp while maintaining a relative low beam energy of several MeV throughout the cavity. As the bunch propagating through VM cavity, the imparted significant velocity modulation is converted to longitudinal density modulation simultaneously. The curvature of the longitudinal phase space is also varied accordingly [see Figs. 1(b) and 1(c)], which is similar with the effect of the energy modulation impacted by a higher harmonic cavity [20] or a dielectric structure [21–23]. In the following drift segment, due to the low beam energy and large velocity spread induced by VM cavity, the conversion from velocity modulation to density modulation is still evident until the bunch is accelerated to high energy in ACC cavity. ACC cavity is typically of high gradient operating at ~0° to improve the beam energy in a short distance and freeze the shaped current profile [see the similar current profiles of Figs. 1(d) and 1(e)]. Figure 1 indicates that if a proper velocity modulation is imposed, the beam can be fixed to a desired profile.

We note that the shaping concept is applicable to both traveling-wave and standing-wave cavities. For the sake of simplicity, VM cavity is supposed to be a traveling-wave structure in this section. Phases of the electron with respect to the wave at different positions are correlated by $\phi^* = \phi_e + \Delta\phi$, where ϕ^* is the electron phase after the drift segment, ϕ_e is the electron phase at the exit of VM cavity, and $\Delta\phi$ is the phase change induced by the L-distance drift segment, which can be expressed as [30]

$$\Delta\phi = k\left(\gamma_e \Big/ \sqrt{\gamma_e^2 - 1} - 1\right)L \approx kL/2\gamma_e^2. \tag{1}$$

Here k is the rf wave number, and the Lorentz factor of the electron at the exit of VM cavity γ_e is invariant during the drift. Given the initial state (γ_0, ϕ_0) at the entrance of VM cavity and the peak electric field E_{peak} of VM cavity, the electron state (γ_e, ϕ_e) can be numerically solved [30–32], for example, using the Runge-Kutta method. Note that ϕ^* can be regarded as a function of ϕ_0, which represents the mapping of the beam longitudinal distributions from the entrance of VM cavity to the end of the drift segment. Adjusting γ_0 (determined by the phase and the amplitude of the gun) and E_{peak} can alter the curvature of the $\phi^*(\phi_0)$ curve, while the injected phase at the entrance of VM cavity ϕ_0 determines which part of the $\phi^*(\phi_0)$ curve taking effect in mapping an input current profile to a shaped profile. By the selection of proper γ_0, E_{peak}, and ϕ_0, the longitudinal beam profile can be shaped to a great extent.

Here a typical operation state of the beamline is considered. The gun is of high gradient operating at 0°, $\gamma_0 = 12$, $E_{\text{peak}} = 8$ MV/m, $L = 7.0$ m, and ACC cavity is operating at 0° with a peak electric field of 24 MV/m. The relative phases at different locations with ϕ_0 are presented in Fig. 2(a). When ϕ_0 is close to 0°, the injected particle is continuously accelerated inside VM cavity and the phase slippage from VM cavity entrance to exit (i.e., $\phi_e - \phi_0$) is relatively small. When ϕ_0 is a decelerating phase, especially when $\phi_0 \ll -90°$, the particle first experiences strong deceleration and then slips to an acceleration phase, thus the phase slippage $\phi_e - \phi_0$ becomes significant. Hence $\phi_e(\phi_0)$ is typically shown to be "V-shaped" with the turning point located at the decelerating region [see the green dashed curve in Fig. 2(a)]. For $\Delta\phi(\phi_0)$, as indicated by Eq. (1) and the shape of $\gamma_e(\phi_0)$ curve [Fig. 2(b)], part of the $\Delta\phi(\phi_0)$ curve appears to be concave, as shown by the purple dotted curve in Fig. 2(a). Here $\Delta\phi(\phi_0)$ is defined to be concave if $d^2(\Delta\phi)/d(\phi_0)^2 < 0$, while defined to be convex if $d^2(\Delta\phi)/d(\phi_0)^2 > 0$. If γ_e is low enough, the concavity of $\Delta\phi(\phi_0)$ can be significant enough to "cancel out" the localized convexity of the corresponding region of $\phi_e(\phi_0)$, so that a concave region can exist in $\phi^*(\phi_0)$ profile [see the black solid curve in Fig. 2(a)].

If a Gaussian-like beam is injected within a concave region of $\phi^*(\phi_0)$, it can be mapped to a nearly linearly ramped distribution. Two examples of mapping Gaussian distributions are shown in Figs. 2(c) and 2(d), representing under-compression mode (the beam tail stays behind the head) and over-compression mode (the beam tail overtakes the head), respectively. It is worth noting that the phase change from the entrance to exit of ACC cavity is almost uniform along the bunch [see the blue dash-dotted curve in Fig. 2(a)], thus the generated profile can be maintained after propagating through ACC cavity.

It needs to be mentioned that all collective effects are neglected in the analysis above. However, under low beam

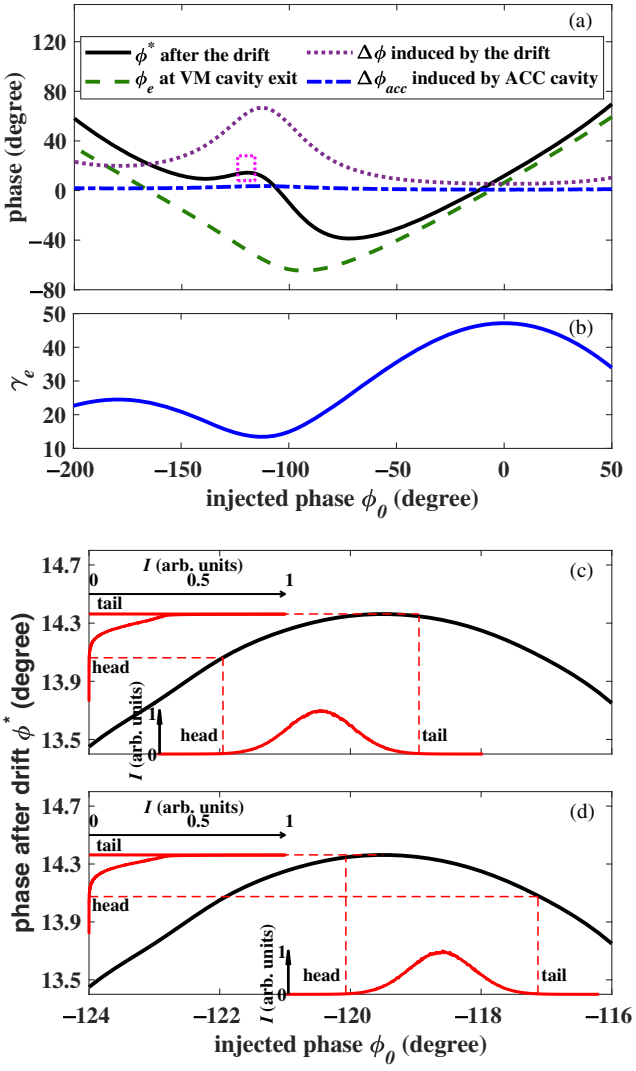

FIG. 2. Examples of mapping a Gaussian distribution to a nearly linearly ramped distribution. (a) Relationships of electron-phase-related quantities ϕ^*, ϕ_e, $\Delta\phi$, and $\Delta\phi_{\text{acc}}$ versus the injected phase at VM cavity entrance ϕ_0. (b) Relationship of γ_e versus ϕ_0. The region surrounded by a pink dotted rectangle in (a) is depicted as black curves in (c) under-compression shaping mode and (d) over-compression shaping mode. The red curves at bottom part of (c) and (d) are current profiles at the entrance of VM cavity, and the red curves at left part are current profiles after the drift segment.

energy and high peak current situations, the space charge effects and the longitudinal wakefield can induce a nonlinear positive energy chirp, which may wash out the negative chirp provided by VM cavity for shaping. As a result, the concave part within $\phi^*(\phi_0)$ may even disappear and the desired triangular profile cannot be obtained. The impact of these collective effects can be alleviated by providing a larger negative chirp within VM cavity, such as adopting a higher E_{peak} or selecting ϕ_0 closer to $-90°$. Particle-tracking simulations show that even the space charge effects and the longitudinal wakefield effect are included, a linearly ramped profile can still be produced by selecting proper drive laser duration and proper amplitudes and phases for the gun and VM cavity.

III. BEAMLINE DESIGN AND SIMULATION FOR A HIGH-CHARGE SHAPED BUNCH

A realistic accelerator beamline configuration is designed to demonstrate the velocity-modulation-based shaping scheme via tracking simulations. The beamline can serve as a bunch-shaping injector, producing high-charge electron bunches with linearly ramped current profile accelerated to 165 MeV. The injector is simulated by program ASTRA with 10^6 macroparticles, and both the space charge effects and the wakefield effects are included.

A block diagram of the injector is shown in Fig. 3(a). The corresponding axial electric field E_z and the magnetic field B_z are plotted in Fig. 3(b). Here a normal conducting 1.3 GHz photocathode gun is adopted for high-charge bunch generation. The gun is enclosed by a special-designed solenoid [33], which can generate an asymmetric

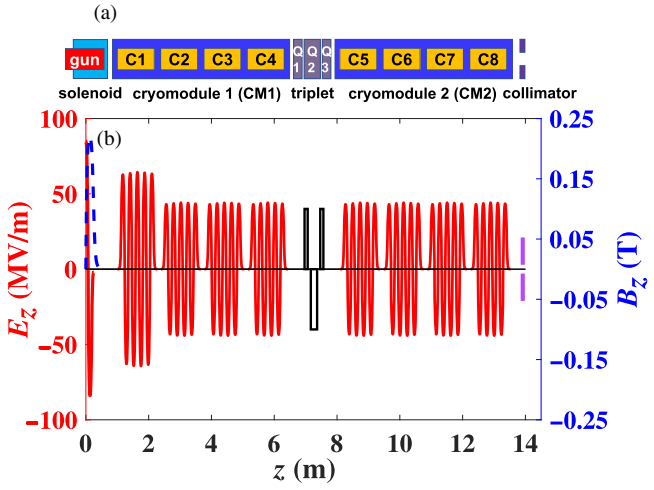

FIG. 3. Configuration of the injector for velocity-modulation-based shaping scheme. (a) A block diagram of elements settings, where C1–C8 denote SRF cavity 1–8, respectively, and Q1–Q3 are quadrupoles. (b) The E_z of cavities (red solid curves) and B_z of the solenoid (blue dashed curve) along the injector. The black boxes denote the position of the triplet, and the purple boxes denote the position of the collimator.

field [see the blue dashed curve in Fig. 3(b)] for emittance compensation. Each of the two accelerator cryomodules [see CM1 and CM2 in Fig. 3(a)] is composed of four TESLA-shape 1.3 GHz nine-cell standing-wave superconducting radio-frequency (SRF) cavities. The quadrupole triplet between two cryomodules is for beam size control. After CM2, a collimator with half gaps of 2.8 mm in both x and y dimensions is applied to scrape off the peripheral particles.

The detailed parameters for the injector are listed in Table I. The laser spot diameter and the gradient of the photocathode gun are selected according to Ref. [34]. The transverse distribution of the laser is 2σ truncated Gaussian, and the temporal distribution is Gaussian. Figure 4 shows the evolution of beam parameters along the injector. Points P, M, and N denote the entrance of cavity 1 [C1 in Fig. 3(a)], the rear part of C1 and the front part of cavity 2 [C2 in Fig. 3(a)], respectively. At point P, the current profile preserves as Gaussian-like. C1 serves as VM cavity in Fig. 1(a), where the beam experiences strong velocity modulation. Along with beam propagation, the velocity modulation is simultaneously converted to longitudinal density modulation, as shown by the sharp variation of the beam length in segment PM [Fig. 4(c)]. At the exit of C1, the beam energy is reduced from 9.5 to 5.3 MeV [Fig. 4(d)], and a large energy spread is introduced [Fig. 4(e)] as expected. Here a high peak gradient of 35 MV/m [35] is adopted to alleviate the space charge effects and the wakefield effects.

As the beam propagating through segment MN, the space charge effects keep significant due to the relatively low beam energy (∼5 MeV) and the short beam length. Consequently, a growth of the normalized emittance can be observed in Fig. 4(a). Further analysis indicates that most of the emittance growth is contributed by the bunch tail, where the collective effects are particularly severe.

TABLE I. Parameters set for the injector.

Parameter	Value	Unit
Initial emitted bunch charge	56	nC
Laser spot diameter	22	mm
Laser duration (rms)	7.45	ps
Thermal emittance (rms)	4.56	mm mrad
rf gun peak electric field	85	MV/m
rf gun phase	−0.5	Degree
C1 peak electric field (E_{acc})	35	MV/m
C2–C8 peak electric field (E_{acc})	24	MV/m
C1 phase	−101.4	Degree
C2–C8 phase	−20	Degree
Solenoid field B_z	0.2204	T
Quadrupole 1/3 strength	1.72	T/m
Quadrupole 2 strength	−1.69	T/m
Collimator half gaps in x/y	2.8	mm
Total length	14	m

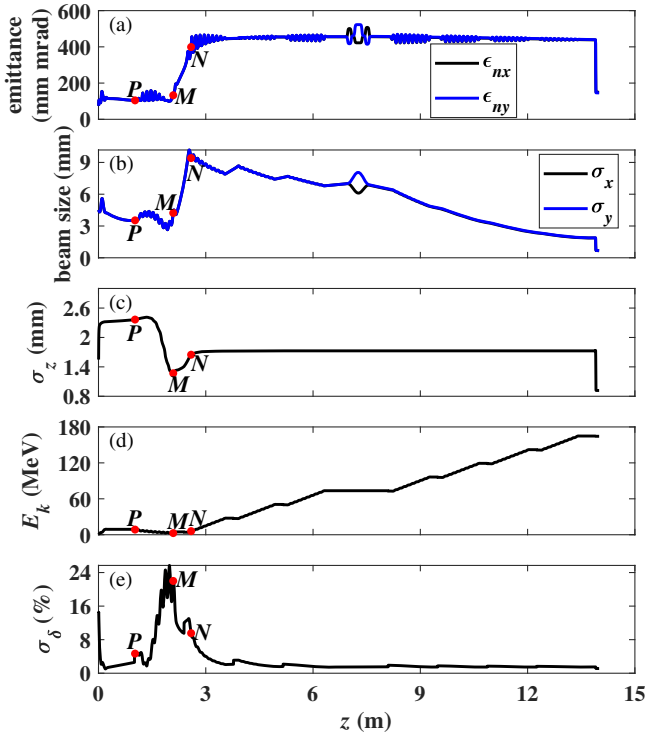

FIG. 4. The evolution of (a) normalized transverse emittance, (b) beam sizes, (c) rms beam length, (d) average kinetic energy, and (e) relative energy spread along the injector, respectively. Point P, M, and N denote the entrance of C1, the rear part of C1 and the front part of C2, respectively.

The sharp growth of beam spot sizes is also observed, as shown in Fig. 4(b). Figure 5 displays the transverse beam profile with a maximum diameter of 59.6 mm reached in the injector. Considering the 70-mm aperture of the adopted cavities and a trajectory instability of 5%–10%, this spot size is acceptable.

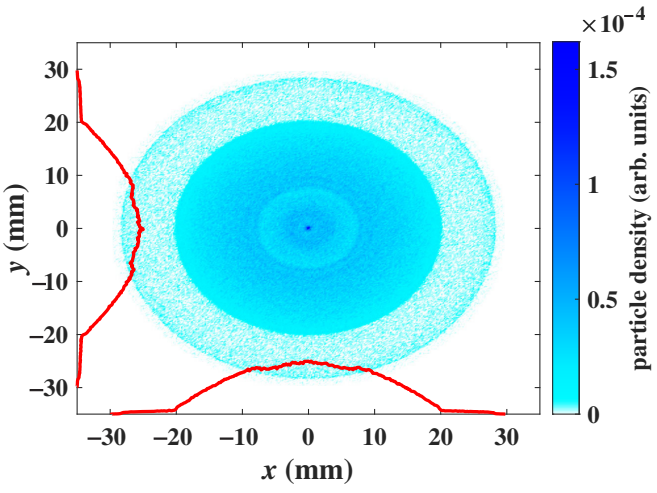

FIG. 5. The maximum beam spot reached in the injector, and the red curves show the transverse beam profiles in x and y dimensions.

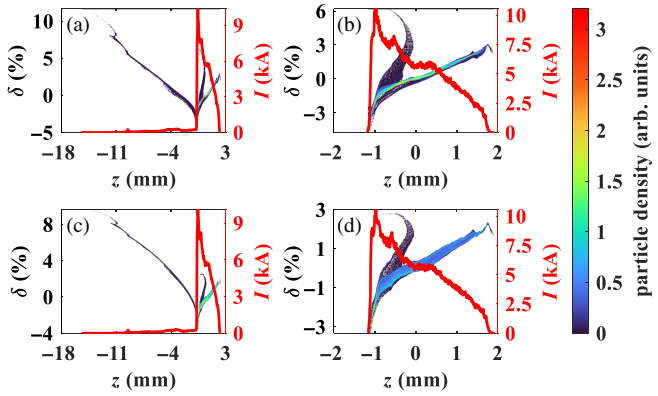

FIG. 6. Longitudinal phase spaces with corresponding current profiles of the whole bunch (a), (c) and the triangular head (b), (d) at the exit of CM1 (a), (b) and CM2 (c), (d), respectively. The bunch head is at right.

C2–C8 are used for energy boosting [serve as ACC cavity in Fig. 1(a)], and the −20° off-crest acceleration is adopted to reduce the energy chirp. A relatively lower gradient of 24 MV/m [9] is adopted here for pursuing higher quality factor Q_0. At the exit of CM1, where the bunch is accelerated to 74 MeV, the emittance and length of the beam are basically "frozen," and a triangular current profile can be observed from Figs. 6(a) and 6(b). At the exit of CM2, the beam is accelerated to 165 MeV and the beam profile is almost unchanged [seen from Figs. 6(c) and 6(d)], revealing that it has been fixed since the exit of CM1. The triangular part of the profile with a peak current over 10 kA contains the charge of >51 nC, as shown in Fig. 6(d).

The phases of the beam particles at the exit of CM2 (ϕ_{out}) versus the injected phases into C1 (ϕ_{in}) is shown in Fig. 7.

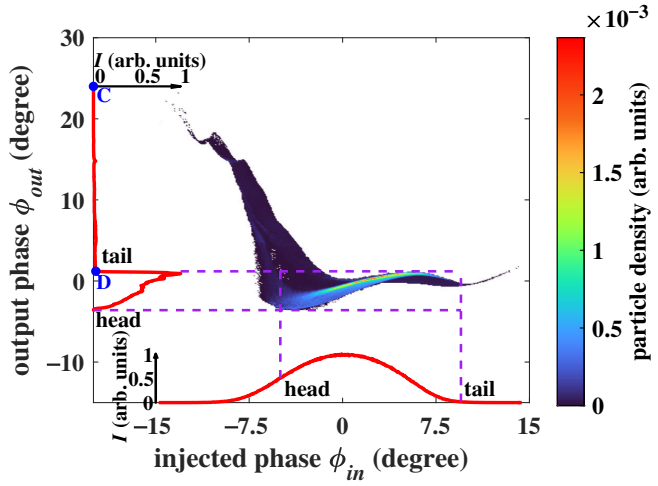

FIG. 7. Phases of beam particles at the exit of CM2 (ϕ_{out}) versus the injected phases into C1 (ϕ_{in}). The red curves denote the current profiles at the entrance of C1 and the exit of CM2. The area surrounded by four purple dashed lines denotes a basically concave region of $\phi_{\text{out}}(\phi_{\text{in}})$.

It turns out that the main part of the injected region of $\phi_{\mathrm{out}}(\phi_{\mathrm{in}})$ is concave. It proves that though the collective effects affect the current profile and impose more restrictions on some parameters (e.g., the requirement for high gradient of C1), suitable parameters can still be found to generate a linearly ramped profile.

A bifurcated longitudinal phase space can be observed in Figs. 6(b) and 6(d). Particle tracking shows that the left branch contains about 3 nC charge and originates from the initial bunch tail. In addition, a long trailing tail can be observed (see "CD" part of the red curve in Fig. 7). Particle tracking shows that it contains 4.8 nC charge and mainly originates from the initial bunch head, which slips backward due to the deceleration in C1. Both the phase space branching and the long trailing tail are principally contributed by the collective effects, which are particularly significant at the bunch head and tail.

For the phase space branching, the discrepancy in relative energy spread between the branches will be narrowed after further accelerated in the main linac, thus it turns out to be not a severe problem for final focusing. For the long trailing tail, most particles are far off the z axis, which can be scraped off by the collimator following CM2. As shown in Fig. 8, after bunch scraping, 50.85 nC charge is still kept in the triangular part, while only 280 pC charge remains in the trailing part. Besides, accompanied with the scraping process, the emittance is also effectively reduced, as shown in Fig. 4(a). Note that the charge-loss rate of 8.7% here is much lower than mask-based shaping scheme [12–17], since the bunch-scraping process is just for tail cutting and emittance control rather than transversely shape of a triangular profile. If further improvement of the shaping quality is needed, a transverse-deflecting-cavity-based collimator for removing tails from the beam longitudinal profile can be considered [36].

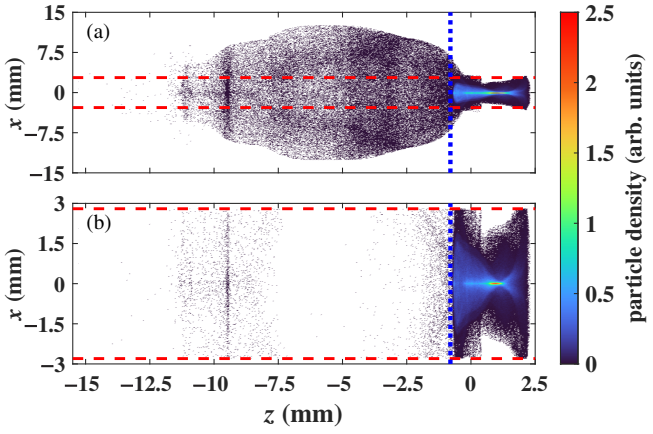

FIG. 8. Diagrams of the beam at the entrance (a) and the exit (b) of the collimator (projected in $x-z$ dimensions, bunch head at right). The red dashed lines denote the gap of the collimator, particles outside which are scraped off. On the right of the blue dotted line is the triangular part of the beam, containing about 50.85 nC charge.

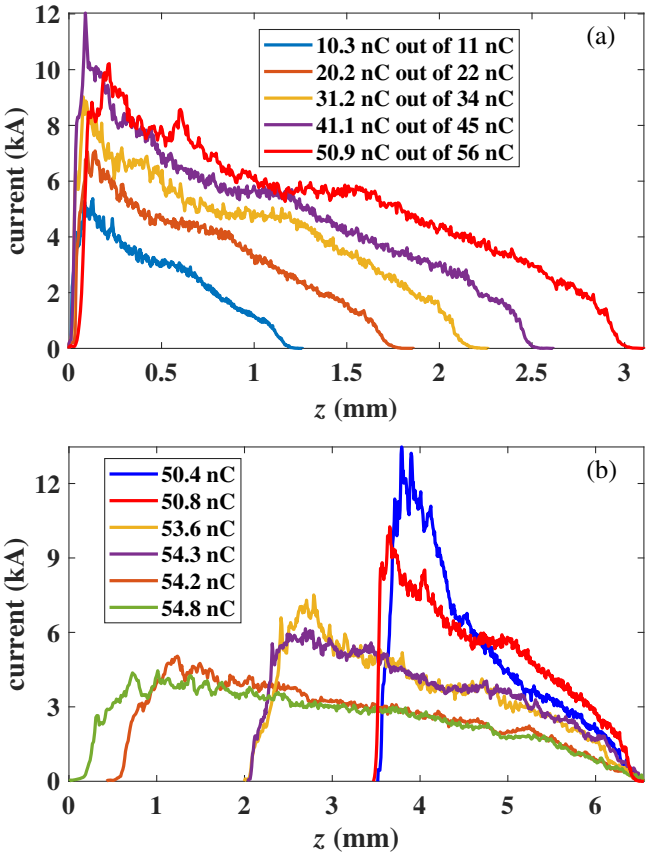

FIG. 9. Linearly ramped current profiles with (a) different bunch charge and (b) different peak current of a 56 nC bunch. Both are at the exit of the injector shown in Fig. 3 and only triangular parts of the bunches are plotted. The bunch heads are at right.

IV. PERFORMANCES ON CHARGE TUNABILITY, PEAK CURRENT TUNABILITY, AND SHAPING ROBUSTNESS

In this section, the charge tunability, the peak current tunability, and the shaping robustness of the proposed shaping scheme are discussed. As shown in Fig. 9, the proposed scheme shows good performance on the tunability of bunch charge and peak current. By adjusting drive laser duration and the amplitudes and phases of the gun and C1, the desired profiles can be produced for different bunch charge [Fig. 9(a)], and the peak current is to a large extent tunable for

TABLE II. Considered jitters of the beamline.

Parameter	Jitter (rms)
Initial emitted bunch charge	2%
Peak electric field of the gun	0.01%
Phase of the gun	0.02°
Strength of the solenoid	0.05%
Peak electric fields of SRF cavities	0.01%
Phases of SRF cavities	0.015°

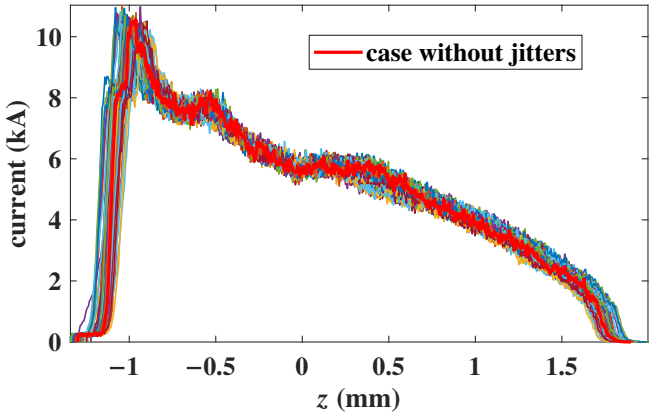

FIG. 10. Current profiles of the ideal case (without jitters) and 100 cases with jitters (bunch heads at right). Here only triangular parts of the bunches are plotted.

a given bunch charge [Fig. 9(b)]. Simulations indicate that the maximum bunch charge or peak current is mainly restricted by the maximum acceptable beam sizes in cavities. For the case shown in Sec. III, the bunch charge or peak current may be further increased by optimization of laser spot at photocathode, replacing C1 with a normal conducting cavity to add solenoids nearby, or adopting larger-aperture SRF cavities (e.g., 650 MHz SRF cavities) in CM1.

Considering the high-charge and low energy features of the proposed shaping scenario, the robustness should also be validated. As mentioned in Sec. III, the linearly ramped profile has been fixed since the exit of CM1, thus only the longitudinal jitter sources before the exit of CM1 are concerned here. 100 simulations of the injector beamline (from the cathode to the exit of CM1) are performed for investigation of the shaping sensitivity to the shot-to-shot jitters, which are randomly generated using a Gaussian probability function with standard deviations listed in Table II. The listed jitter values are referred to state-of-the-art accelerator technology [9,28,35,37].

Figure 10 presents the current profiles of the ideal case (without jitters) and 100 cases with jitters. It indicates that a stable current profile can be maintained. It is worth noting that the strict control of the amplitude/phase jitters is only necessary in cavities in CM1 (in particular, C1 and C2), where the energy is still not high and the current profile is not fully "frozen." Thus the subsequent cavities have more tolerance on jitters and can gain more freedom on optimization of beam quality.

V. APPLICATION TO HIGH-TRANSFORMER RATIO PWFA

In this section, the performance of a >50 nC high-energy shaped beam to drive HTR PWFA is validated. The shaped beam obtained from the end of the injector is imported to a main linac for energy boosting and final focusing, and then serves as a drive beam for PWFA. The particle tracking in the main linac is simulated by ELEGANT [38], including longitudinal space charge effects and wakefield effects. The main linac is composed of a matching section, six periodical accelerating-matching sections, and a final focusing system, as shown in Fig. 11(a). Each periodical section includes a cryomodule and a quadrupole doublet, and each cryomodule includes eight TESLA-shape 1.3 GHz nine-cell SRF cavities with E_{acc} of 22 MV/m. Due to the strong longitudinal wakefield for such a high-current bunch, −40° off-crest acceleration is applied to compensate the wake-induced energy chirp. At the end of the main linac, the energy is boosted to 1 GeV, and the bunch is focused to 93 μm (rms) transversely with normalized emittance of 102 mm mrad. Figure 11 shows the evolution of the beam parameters along the main linac. The longitudinal phase space with corresponding current profile of the bunch at the end of the main linac are shown in Fig. 12, revealing that the current profile remains unchanged during the propagation through the main linac.

The bunch obtained at the end of the main linac is exported to QuickPIC [39,40] as the input for demonstration of HTR PWFA. Note that the charge of the bunch tail is only 0.6% of the triangular part, and the twiss parameter β of the bunch tail is several times greater than that of the

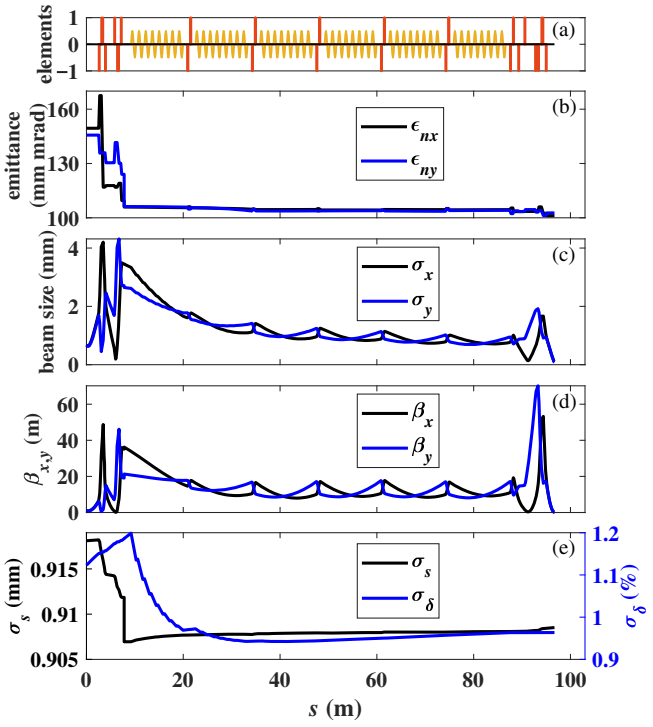

FIG. 11. Lattice design (a) and the evolution of the (b) normalized transverse emittance, (c) beam sizes, (d) beta functions, and (e) rms beam length and relative energy spread along the main linac. The red boxes and golden curves denote quadrupoles and accelerating cavities respectively. Note that before accelerated in the main linac, another collimator is applied for emittance control (not plotted), leading to 380 pC charge loss.

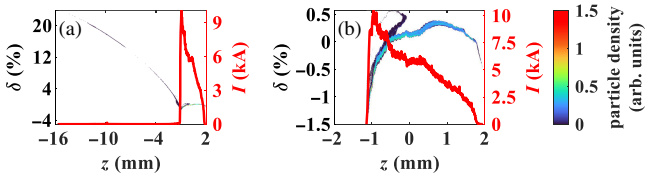

FIG. 12. Longitudinal phase space with corresponding current profile of the whole bunch (a) and its triangular head with 50.44 nC charge (b) at the end of the main linac. The bunch head is at right.

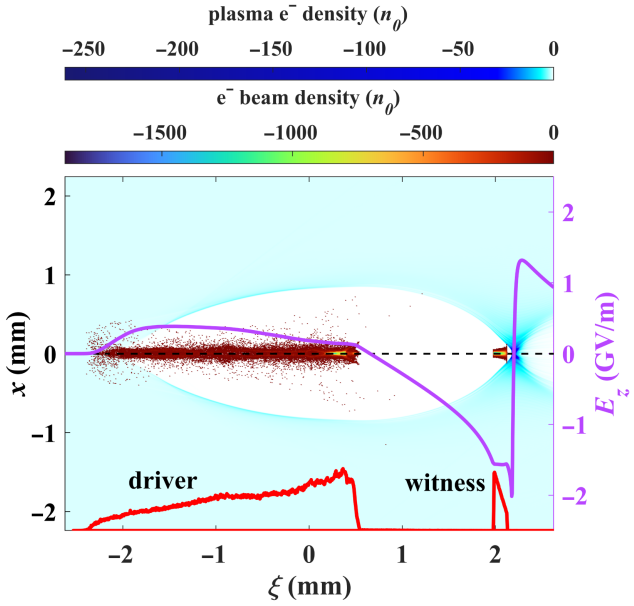

FIG. 13. Cross sections of the beam and plasma electron density distributions (in unit of $n_0 = 1.4 \times 10^{14}$ cm^{-3}), current profiles of the drive beam and witness beam (red curves), and on-axis electric field E_z (purple curve) in the uniform plasma. ξ denotes the relative longitudinal positions of the beam particles. The bunch head is at left.

triangular part. The bunch tail is thus expected to have little effect on PWFA and most of its particles will loss due to the large β. Here a uniform plasma section with a density of 1.4×10^{14} cm^{-3} is adopted and only the particles in the first plasma bubble (50.62 nC) are considered in simulation. A >3 nC witness beam with inverted trapezoidal current profile is loaded to make the accelerating field flat. As shown in Fig. 13, the maximum decelerating gradient experienced by the drive beam is 0.385 GV/m, and the maximum accelerating gradient experienced by the witness beam is 1.553 GV/m, leading to the transformer ratio of 4.03. The transformer ratio is expected to be further improved if making more refinements on the bunch head (e.g., generation of a doorstep distribution [4]), which is the subject of future dedicated studies. Note that due to the high peak current of the drive bunch, the witness beam can be generated in a plasma-based injector, such as density-downramp injection [41].

VI. SUMMARY

In this paper, a CSR-free scheme of manipulating the longitudinal bunch profile by velocity modulation is proposed, and its capability to generate a shaped bunch with charge of >50 nC and charge-loss rate of <10% is demonstrated via start-to-end simulations. The proposed shaping scheme is also presented to be charge-tunable, peak current-tunable, and robust by further analysis. Finally, the high-charge shaped bunch with a linearly ramped current profile is numerically demonstrated to be capable of loading a 3 nC witness bunch and producing a transformer ratio larger than 4 with an accelerating wakefield over GV/m in plasma. Future work is still required to investigate the beam dynamics at low energy region in detail, explore new methods to deal with the long trailing tail or charge loss, and generate better bunch profile for improvement of the transformer ratio.

ACKNOWLEDGMENTS

The authors are grateful to Dr. Han Chen (THU), Dr. Zhichao Dong (THU), Dr. Zheng Zhou (CAEP), and Dr. Kui Zhou (CAEP) for useful materials and discussions. This work is supported by the Strategic Priority Research Program of the Chinese Academy of Sciences (Grant No. XDB0530000), the National Natural Science Foundation of China (Grants No. 11991071, No. 12375241, No. 12305152, and No. 11991073), Discipline Construction Foundation of "Double World-class Project" and the National Science and Technology Major Project (Grant No. 2019-VII-0019-0161). The simulation work is supported by the Center of High Performance Computing, Tsinghua University.

[1] P. Chen, J. M. Dawson, R. W. Huff, and T. Katsouleas, Acceleration of electrons by the interaction of a bunched electron beam with a plasma, Phys. Rev. Lett. **54**, 693 (1985).

[2] I. Blumenfeld, C. E. Clayton, F.-J. Decker, M. J. Hogan, C. Huang, R. Ischebeck, R. Iverson, C. Joshi, T. Katsouleas, N. Kirby, W. Lu, K. A. Marsh, W. B. Mori, P. Muggli, E. Oz, R. H. Siemann, D. Walz, and M. Zhou, Energy doubling of 42 GeV electrons in a metre-scale plasma wakefield accelerator, Nature (London) **445**, 741 (2007).

[3] M. Litos *et al.*, High-efficiency acceleration of an electron beam in a plasma wakefield accelerator, Nature (London) **515**, 92 (2014).

[4] K. L. F. Bane, P. Chen, and P. B. Wilson, On collinear wake field acceleration, IEEE Trans. Nucl. Sci. **32**, 3524 (1985).

[5] P. Chen, J. J. Su, J. M. Dawson, K. L. F. Bane, and P. B. Wilson, Energy transfer in the plasma wake-field accelerator, Phys. Rev. Lett. **56**, 1252 (1986).

[6] W. Lu, W. An, C. Huang, C. Joshi, W. Mori, M. Hogan, T. Raubenheimer, and A. Seryi, High transformer ratio PWFA for application on XFELs, in *Proceedings of the Particle*

Acellerator Conference, PAC-2009, Vancouver, BC, Canada (IEEE, Piscataway, NJ, 2010), p. WE6RFP098.

[7] Q. Su, J. Larson, T. N. Dalichaouch, F. Li, W. An, L. Hildebrand, Y. Zhao, V. Decyk, P. Alves, S. M. Wild, and W. B. Mori, Optimization of transformer ratio and beam loading in a plasma wakefield accelerator with a structure-exploiting algorithm, Phys. Plasmas **30**, 053108 (2023).

[8] C. Joshi, S. Corde, and W. B. Mori, Perspectives on the generation of electron beams from plasma-based accelerators and their near and long term applications, Phys. Plasmas **27**, 070602 (2020).

[9] The CEPC Study Group, CEPC Technical Design Report–Accelerator (v2), Institute of High Energy Physics (IHEP), Technical Report No. IHEP-CEPC-DR-2023-01, No. IHEP-AC-2023-01, 2023, http://cepc.ihep.ac.cn/CEPC_tdr.pdf.

[10] G. Ha, K.-J. Kim, J. G. Power, Y. Sun, and P. Piot, Bunch shaping in electron linear accelerators, Rev. Mod. Phys. **94**, 025006 (2022).

[11] P. Piot, Y.-E. Sun, J. G. Power, and M. Rihaoui, Generation of relativistic electron bunches with arbitrary current distribution via transverse-to-longitudinal phase space exchange, Phys. Rev. ST Accel. Beams **14**, 022801 (2011).

[12] B. Jiang, C. Jing, P. Schoessow, J. Power, and W. Gai, Formation of a novel shaped bunch to enhance transformer ratio in collinear wakefield accelerators, Phys. Rev. ST Accel. Beams **15**, 011301 (2012).

[13] G. Ha, M. H. Cho, W. Namkung, J. G. Power, D. S. Doran, E. E. Wisniewski, M. Conde, W. Gai, W. Liu, C. Whiteford, Q. Gao, K.-J. Kim, A. Zholents, Y.-E. Sun, C. Jing, and P. Piot, Precision control of the electron longitudinal bunch shape using an emittance-exchange beam line, Phys. Rev. Lett. **118**, 104801 (2017).

[14] Q. Gao, G. Ha, C. Jing, S. P. Antipov, J. G. Power, M. Conde, W. Gai, H. Chen, J. Shi, E. E. Wisniewski, D. S. Doran, W. Liu, C. E. Whiteford, A. Zholents, P. Piot, and S. S. Baturin, Observation of high transformer ratio of shaped bunch generated by an emittance-exchange beam line, Phys. Rev. Lett. **120**, 114801 (2018).

[15] R. Roussel, G. Andonian, W. Lynn, K. Sanwalka, R. Robles, C. Hansel, A. Deng, G. Lawler, J. B. Rosenzweig, G. Ha, J. Seok, J. G. Power, M. Conde, E. Wisniewski, D. S. Doran, and C. E. Whiteford, Single shot characterization of high transformer ratio wakefields in nonlinear plasma acceleration, Phys. Rev. Lett. **124**, 044802 (2020).

[16] G. Ha, J. G. Power, J. Shao, M. Conde, and C. Jing, Coherent synchrotron radiation free longitudinal bunch shaping using transverse deflecting cavities, Phys. Rev. Accel. Beams **23**, 072803 (2020).

[17] R. J. England, C. K. Ng, J. Frederico, M. J. Hogan, M. Litos, P. Muggli, C. Joshi, W. An, G. Andonian, W. Mori, and W. Lu, High transformer ratio drive beams for wakefield accelerator studies, AIP Conf. Proc. **1507**, 553 (2012).

[18] R. J. England, J. B. Rosenzweig, G. Andonian, P. Musumeci, G. Travish, and R. Yoder, Sextupole correction of the longitudinal transport of relativistic beams in dispersionless translating sections, Phys. Rev. ST Accel. Beams **8**, 012801 (2005).

[19] R. J. England, J. B. Rosenzweig, and G. Travish, Generation and measurement of relativistic electron bunches characterized by a linearly ramped current profile, Phys. Rev. Lett. **100**, 214802 (2008).

[20] P. Piot, C. Behrens, C. Gerth, M. Dohlus, F. Lemery, D. Mihalcea, P. Stoltz, and M. Vogt, Generation and characterization of electron bunches with ramped current profiles in a dual-frequency superconducting linear accelerator, Phys. Rev. Lett. **108**, 034801 (2012).

[21] G. Andonian, F. O'Shea, S. Barber, and J. Rosenzweig, Bunch profile shaping using beam self-wakefields in a dielectric structure, AIP Conf. Proc. **1777**, 070002 (2016).

[22] G. Andonian, S. Barber, F. H. O'Shea, M. Fedurin, K. Kusche, C. Swinson, and J. B. Rosenzweig, Generation of ramped current profiles in relativistic electron beams using wakefields in dielectric structures, Phys. Rev. Lett. **118**, 054802 (2017).

[23] Z. Dong, H. Chen, C. Song, Y. Tan, Q. Tian, H. Zhang, Z. Zhou, Z. Li, Y. Du, R. Li, L. Yan, W. Huang, and C. Tang, Longitudinal phase space manipulation with planar corrugated wakefield structures, Nucl. Instrum. Methods Phys. Res., Sect. A **987**, 164819 (2021).

[24] G. Loisch, J. Good, M. Gross, H. Huck, I. Isaev, M. Krasilnikov, O. Lishilin, A. Oppelt, Y. Renier, F. Stephan, R. Brinkmann, F. Grüner, and I. Will, Photocathode laser based bunch shaping for high transformer ratio plasma wakefield acceleration, Nucl. Instrum. Methods Phys. Res., Sect. A **909**, 107 (2018).

[25] G. Loisch *et al.*, Observation of high transformer ratio plasma wakefield acceleration, Phys. Rev. Lett. **121**, 064801 (2018).

[26] F. Lemery and P. Piot, Tailored electron bunches with smooth current profiles for enhanced transformer ratios in beam-driven acceleration, Phys. Rev. ST Accel. Beams **18**, 081301 (2015).

[27] T. Xu, C. Jing, A. Kanareykin, P. Piot, and J. Power, Optimized electron bunch current distribution from a radio-frequency photo-emission source, in *Proceedings of the 2018 IEEE Advanced Accelerator Concepts Workshop (AAC), Breckenridge, CO* (IEEE, New York, 2018), pp. 1–5.

[28] W. H. Tan, P. Piot, and A. Zholents, Formation of temporally shaped electron bunches for beam-driven collinear wakefield accelerators, Phys. Rev. Accel. Beams **24**, 051303 (2021).

[29] K. Floettmann, *ASTRA-A Space Charge Tracking Algorithm* (Deutsches Elektronen-Synchrotron, Hamburg, Germany, 2017).

[30] D. Wang, L. Yan, Y. Du, W. Huang, W. Gai, and C. Tang, Theoretical analysis and simulation study of the deep overcompression mode of velocity bunching for a comb-like electron bunch train, Phys. Rev. Accel. Beams **21**, 024403 (2018).

[31] L. Serafini and M. Ferrario, Velocity bunching in photo-injectors, AIP Conf. Proc. **581**, 87 (2001).

[32] S. Anderson, P. Musumeci, J. Rosenzweig, W. Brown, R. England, M. Ferrario, J. Jacob, M. Thompson, G. Travish, A. Tremaine, and R. Yoder, Velocity bunching of high-brightness electron beams, Phys. Rev. ST Accel. Beams **8**, 014401 (2005).

[33] H. Xu, J. Shi, Y. Du, R. Li, Q. Xing, H. Chen, C. Tang, and W. Huang, Development of an L-band photocathode rf gun at Tsinghua University, Nucl. Instrum. Methods Phys. Res., Sect. A **985**, 164675 (2021).

[34] E. E. Wisniewski, S. P. Antipov, M. Conde, D. S. Doran, W. Gai, C. Jing, W. Liu, J. G. Power, and C. Whiteford, Cs2Te photocathode performance in the AWA high-charge high-gradient drive gun, in *Proceedings of 6th International Particle Accelerator Conference, IPAC-2015, Richmond, VA*, (JACoW, Geneva, Switzerland, 2015), Vol. 6, pp. 3283–3285.

[35] C. Adolphsen, The International Linear Collider Technical Design Report—Volume 3.I: Accelerator R&D in the Technical Design Phase, Argonne National Laboratory (ANL), Argonne, IL; Thomas Jefferson National Accelerator Facility (TJNAF), Newport News, VA; Brookhaven National Laboratory (BNL), Upton, NY; SLAC National Accelerator Laboratory, Menlo Park, CA; Fermi National Accelerator Laboratory (FNAL), Batavia, IL, Technical Report No. ILC-REPORT-2013-040; ANL-HEP-TR-13-20; BNL-100603-2013-IR; IRFU-13-59; CERN-ATS-2013-037; Cockcroft-13-10; CLNS 13/2085; DESY 13-062; FERMILAB TM-2554; IHEP-AC-ILC-2013-001; INFN-13-04/LNF; JAI-2013-001; JINR E9-2013-35; JLAB-R-2013-01; KEK Report 2013-1; KNU/CHEP-ILC-2013-1; LLNL-TR-635539; SLAC-R-1004; ILC-HiGrade-Report-2013-003, 2013, https://linearcollider.org/files/images/pdf/Accelerator.pdf.

[36] E. Kur, G. Penn, J. Qiang, M. Venturini, R. Wells, and A. Zholents, Accelerator Design Study for a Soft X-Ray Free Electron Laser at the Lawrence Berkeley National Laboratory, Report No. LBNL-2670E, 2009.

[37] Z. Zhao, D. Wang, Q. Gu, L. Yin, M. Gu, Y. Leng, and B. Liu, Status of the SXFEL facility, Appl. Sci. **7**, 607 (2017).

[38] M. Borland, ELEGANT: A flexible SDDS-compliant code for accelerator simulation, Argonne National Laboratory, IL, Technical Report No. LS-287, 2000.

[39] C. Huang, V. K. Decyk, C. Ren, M. Zhou, W. Lu, W. B. Mori, J. H. Cooley, T. M. Antonsen, and T. Katsouleas, QUICKPIC: A highly efficient particle-in-cell code for modeling wakefield acceleration in plasmas, J. Comput. Phys. **217**, 658 (2006).

[40] W. An, V. K. Decyk, W. B. Mori, and T. M. Antonsen, An improved iteration loop for the three dimensional quasi-static particle-in-cell algorithm: QuickPIC, J. Comput. Phys. **250**, 165 (2013).

[41] H. Suk, N. Barov, J. Rosenzweig, and E. Esarey, Plasma electron trapping and acceleration in a plasma wake field using a density transition, Phys. Rev. Lett. **86**, 1011 (2001).